Pa-Count: Passenger Counting in Vehicles Using Wi-Fi Signals

Hongbo Jiang ⓘ, *Senior Member, IEEE*, Siyu Chen ⓘ, Zhu Xiao ⓘ, *Senior Member, IEEE*, Jingyang Hu ⓘ, Jiangchuan Liu ⓘ, *Fellow, IEEE*, and Schahram Dustdar ⓘ, *Fellow, IEEE*

Abstract—Passenger counting is crucial for many applications such as vehicle scheduling and traffic capacity assessment. However, most of the existing solutions are either high-cost, privacy invasive or not suitable for passengers the vehicle scenarios. In this work, we propose the Pa-Count, an effective real-time Passenger Counting system deployed inside the vehicle via using Wi-Fi *CSI* (Channel State Information). Specifically, in Pa-Count, we design a set of combined filters to eliminate environmental interference and enhance CSI quality. In so doing, we can identify the fluctuation of weak CSI caused by passengers' subtle movement, i.e., the fidgeting, and then obtain the distribution of fidgeting period and silent period. Following that, we describe the subtle movements of passengers via power law with exponential cutoff distribution and establish a counting model based on the queuing theory. A mathematical inference method with a priori probability is devised to calculate the number of real-time passengers through CSI. We evaluate the performance of the Pa-Count by conducting a set of experiments in real-world vehicle scenarios (including private car and subway). Experimental results show that Pa-Count can achieve robust performance with an average accuracy of over 92%.

Index Terms—Wi-Fi sensing, passenger counting, queuing theory.

I. INTRODUCTION

NOWADAYS, more and more people travel and commute in urban regions by using various vehicles, such as passenger

cars (e.g., private car and taxi) and public transportation (e.g., bus and subway) [1], [2], [3]. Real-time passenger counting in vehicles is important to auto manufacturers and transportation operators. More specifically, knowing the number of passengers in private car can provide vehicle manufacturers the passengers' riding habits, which is helpful to better plan future products [4], [5]. Based on the real-time passenger numbers, the operators of taxis and carpooling [6], [7] can better dispatch orders, thereby shortening the waiting time for passengers and improving the revenue of drivers. For public transportation, the number of passengers in the bus at different periods plays a significant role in the real-time scheduling of vehicles by the traffic management department. Besides, counting passengers enables passenger flow monitoring, helping to assess and predict the dynamic capacity risk of public transport networks [8]. In the subway, real-time passenger counting facilitates resource allocation (such as air conditioners, empty seats, etc.), and subway passenger flow detection can support decision-making for sustainable urban development [9].

Existing studies for passenger counting include wearable device-based methods, acoustic-based methods, visible light and imagery-based methods and radio frequency signals based methods. Wearable device-based methods for counting aim to detecting human biometrics (e.g., heartbeat, breathing and other information [10], [11]). The feasibility of such methods is limited as they rely on the passengers wearing devices and their willingness to open access to biometric data. Acoustic signals [12] are susceptible to the environmental interference and multipath effect in vehicles. Visible light and imagery [13], [14], [15] are widely used for crowd counting. These methods can achieve high accuracy without too many restrictions on passengers. However, using optical sensors requires high-cost equipment, and the use of cameras may bring privacy concerns for the passengers. Radio frequency signals include radar signals and Wi-Fi signals. Radar detects and analyzes the echo reflected from the target [16]. However, the human body is a very complex reflector, the accuracy of the existing compact commercial radars cannot detect the weak movement of the passenger in the vehicle [17]. Existing methods using Wi-Fi signals are mainly implemented by received signal strength indicator (RSSI) and channel state information (CSI). Although many studies have focused on counting using RSSI signal [18], [19], the accuracy of RSSI signal is low because the multipaths cause unpredictable RSSI fluctuations. Thanks to the advantages of Wi-Fi CSI signals that can effectively overcome

the influence of the environment and multipath effects, crowd number detection based on CSI signals has emerged, and [20], [21], [22] show high robustness and accuracy by using Wi-Fi CSI signals.

Although the crowd counting based on Wi-Fi CSI signals has been well developed, counting passengers in a moving vehicle by Wi-Fi CSI signals face the following challenges. *i)* How to effectively capture weak signals caused by subtle movements of passengers in a moving vehicle? The basis of counting through wireless signals is to detect the signal fluctuations that are caused by the movements of objects. Whereas the passengers' subtle movements (what we call '*fidgeting*') are much slighter than common human movements, thus the signal fluctuations caused by fidgeting are quite weak. Moreover, the environmental interference in a moving vehicle, which is generated by vehicle starts, pauses and bumps, hinders the capture of weak signal.

ii) How to resolve the overlapped signals caused by the fidgeting from multiple passengers? The fidgeting movement of multiple passengers have accumulative effects [23] on the received Wi-Fi CSI signals. One way to deal with overlapping signals is signal separation. Most of the existing Wi-Fi bandwidths are less than 300 MHz, consequently the range resolution (c/2B, c is the speed of light and B is the bandwidth) is no more than 0.5 m, and it's common for passengers to be within 0.5 m of each other in the vehicle. The received signals cannot be easily de-coupled. The other method is to analyze the signal through statistics. For instance, [24] tried to resolve the overlapped signal through queuing theory model. However, the Poisson distribution used in [24] no longer accurately describes passenger fidgeting in the moving vehicle scenarios.

To address the above-mentioned challenges, we develop the Pa-Count, an effective real-time Passenger Counting method which can well apply into the moving vehicles. To specify, we propose an efficient design of a time-frequency filter bank in the Pa-Count, which not only eliminates environmental interference, but also enhances the fine-grained signal feature. In so doing, the Pa-Count can detect the subtle movements of passengers in the vehicles. Many existing works have studied the relationship between the subtle movements and the number, while the methods rely on distribution functions in specific scene. In the moving vehicles, these distribution functions will be biased, which cannot be eliminated directly by prior knowledge. To resolve this issue, we derive that the passengers fidgeting in vehicles follows a special power low with exponential cutoff distribution. This distribution can be used to correlate overlapping signals with the number of passengers. To summarize, this work makes the following contributions.

- We design a set of combined filters to eliminate environmental interference and enhance signal quality. We investigate the distribution of environmental interference in the frequency domain and then design a high-pass filter with a cutoff frequency of 20 Hz to remove the interference in the weak Wi-Fi CSI signals. Following that, we utilize the Savitzky-Golay filters based on local polynomial least squares fitting in the time domain, so as to smooth the data by fitting consecutive subsets of adjacent data points to a low-degree polynomial by linear least squares. As such,

the Pa-Count can extract passengers' fidgeting information, i.e., detect the subtle movements, from environmental interference in a moving vehicle.

- We develop a new distribution, namely, a power law with exponential cutoff distribution, to represent the time interval. Such new distribution is more suitable than the Poisson distribution [24] to describe passengers' subtle movements in the vehicle. Depending on this distribution, we build a new passenger counting model. Further, we confirm it by calculating the Kullback-Leibler Divergence.

- We conduct a comprehensive evaluation of the Pa-Count through a series of simulations and field studies. Experimental results show that Pa-Count can achieve robust performance with an average accuracy higher than 92%. Compared with counting passengers using Poisson distribution, our method improves the accuracy, and we raise the measurement limit to 15 passengers. The results show that Pa-Count has better robustness and accuracy than other methods for passenger counting in vehicles.

The remainder of this paper is organized as follows. Section II introduces the state-of-the-art literature on people counting detection and Wi-Fi-based sensing. Section III presents the principle of applying Wi-Fi signals for fidgeting sensing. Section IV presents the implementation of Pa-Count. Section V presents the system evaluation. Section VI discusses the conclusion followed by a limitation of our work.

II. RELATED WORK

In this section, we briefly introduce the literature on passenger counting, including wearable device-based methods, acoustic-based methods, methods based on visible light and imagery, methods based on wireless signal. *Wearable device-based methods.* These methods use breathing sensors and acceleration sensors to obtain biological information such as breathing, heartbeat, and limb movements, and count people based on those biological information. Daniel et al. [25] propose a real-time crowd counting system based on temporary ID broadcasts broadcast by contact tracing applications on wearable devices. Wang et al. [11] propose a method for identifying and counting by estimating respiratory rates. The authors exploit the channel state information (CSI) of a single pair of commercial Wi-Fi devices, and then propose a novel system that can continuously track the breathing rate of multiple people. Despite achieving high accuracy, wearable device-based methods are not suitable for practical scenarios such as in vehicles due to the need to wear wearable devices on the passengers.

Acoustic-Based Methods. Since the acoustic-based methods can be easily implemented by smartphones, these methods have many applications in human perception. For instance, the authors in [12] propose to detect driver behavior using acoustic signals. [26] shows a new gesture recognition approach for clothing-based gesture using active and passive acoustic sensing. However, the acoustic signal is susceptible to external interference. Besides, at the presence of multi-path effect, the acoustic signals remain difficulty to be resolved and hence result in a low upper limit of the number of passengers.

TABLE I
SUMMARY OF THE MAIN NOTATIONS

Notations	Definitions
$t_i^{\{n\}}$	The start of the i-th fidget of the n-th passenger
$d_i^{\{n\}}$	The time duration of the i-th fidget of the n-th passenger
$T_i^{\{n\}}$	i-th interval time of the n-th passenger
$\lambda^{\{n\}}$	n-th passengers average incidence of fidgeting per unit time
$\overline{\lambda}$	all passengers average incidence of fidgeting per unit time
$\overline{T_i}$	the i-th interval time of all passengers
$N_f(t)$	The total number of these fidgeting periods
$N_s(t)$	The total number of such silent periods
$\widehat{N}(t)$	The estimate of the number of passenger at time t

Fig. 1. Overview of Pa-Count.

Methods Based on Visible Light and Imagery. Early visible light and imagery approaches mainly utilize the camera and model the background through a mixture of Gaussian models [27] or identify passengers through explicit shape analysis [28]. As those methods are challenging to apply into cluttered scenes, researchers have turned their attention to machine learning methods. as discussed by Soviany and Ionescu [29], recent advances on deep learning achieve object detection/classification in an image with satisfied performance. Zhang et al. [14] report a method based on Tiny Yolo, to detect people entering/leaving a bus by training a model on the upper body parts of passengers. Liu et al. [15] report a method to measure passenger flows in metros using Yolov3 optimizing its anchors and thus obtaining flow accuracy of 95%. Filipic et al. [13] propose the use of convolutional neural networks (CNN) for counting and positioning people given aerial shots of visible and infrared images. Amin et al. [30] use a neural network to perform crowd density estimation on visible images using a combination of visual and infrared images. Choi et al. [13] propose technique incorporates modified CLEAN-based features in the range domain and energy-based features in the frequency domain to efficiently address both dense and dispersed distributions of individuals. Existing visible light and imagery counting methods are mature, and the performance of detectors and trackers is very good as well. The biggest concern is that these methods may violate the privacy of passengers, and bring a huge amount of computation for accurate identification of crowd.

Radio Frequency Signals Based Methods In these methods, the radio frequency signals are the millimeter wave emitted by radar equipment, and the RSSI signals and CSI signals emitted by Wi-Fi, Bluetooth, LoRa network, etc. Radar signals are often aimed at moving crowd [16] [31]. Using RF signal to monitor human motion and posture is likely infeasible, since human body is a very complex reflector [32]. In [33], the device-free human presence detection method based on 2.4 GHz Zigbee RSSI variations is proposed. Wei et al. [20] design the FCC, a device-Free Crowd Counting approach based on Wi-Fi CSI signal. Inspired by this, we design the passenger counting method by using Wi-Fi CSI signals. Our proposed method can detect the weak fidgeting motion of passengers in a moving vehicle and count passengers by processing overlapping signals.
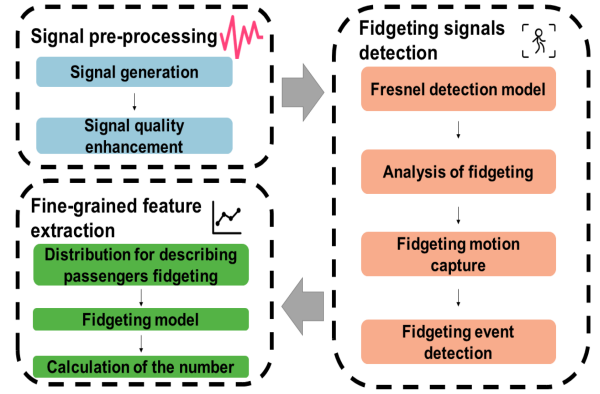
III. PA-COUNT DESIGN

A. System Overview

The design of Pa-Count is to implement real-time passenger counting in vehicles through CSI signals. To specify, the Pa-Count generates Wi-Fi signals and detects the fluctuation of Wi-Fi CSI signals that are caused by the subtle movement, i.e., the fidgeting of passengers. In this line, the Pa-Count can identify the passengers via capturing their fidgeting. Beyond that, Pa-Count uses Power law with exponential cutoff distribution to describe passengers' fidgeting, and builds counting model based on this distribution and queuing theory. The workflow of Pa-Count is presented in Fig. 1.

Signal Pre-Processing. In a moving vehicle, signal fluctuation caused by fidgeting is weak. Besides, there are much environmental interference hindering effective detection of signals from passengers' fidgeting. To resolve this problem, in the Pa-Count, we perform signal pre-processing to eliminate environmental interference and increase the signal granularity to facilitate fidgeting detection. To that end, the generated signal of Pa-Count is the ping packet specified by the 802.11 Wi-Fi standard. Pa-Count eliminates the environmental interference through a high-pass filter and enhance the signal granularity through a Savitzky-Golay filter.

Fidgeting Detection. In Pa-Count, we set a pair of antennas that form a Fresnel zone. Passengers' fidgeting will affect the propagation of the signal and cause signal fluctuations. First, Pa-Count analyzes the characteristics of signal fluctuation caused by fidgeting, then carries out fidgeting motion capture through Fresnel zone model. Finally, it detects fidgeting event through sliding window based on variance threshold. Thus far, we obtain the ratio of fidgeting period and silent period, which is expressed as 0/1 signal.

Passenger Counting. After fidgeting detection, the obtained signals are required to be mapped to the number of passengers. Existing studies such as [24] are unable to apply into the scenario of moving vehicles. Pa-Count designs and verifies a Power law with exponential cutoff distribution function which is consistent with the features of passenger's fidgeting. With such distribution, Pa-Count establishes a counting model based on queuing theory. Combined with prior knowledge, Pa-Count can calculate the number through the Maximum A Posteriori estimation.
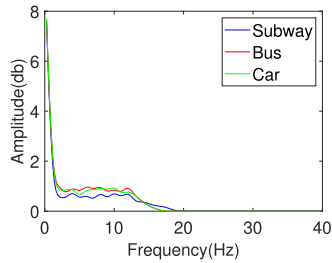
Fig. 2. Frequency distribution of interference.

Fig. 3. The denoised CSI signal.

B. Signal Pre-Processing

1) Signal Generation: The proposed Pa-Count consists of an X310 device [34] and two antennas. The X310 device has independent receiving and transmitting channels, hence it can work in full duplex mode. The radio chip AD9363 in X310 is a high-performance and integrated RF agile transceiver based on a direct conversion receiver. The adjustable range of AD9363 is specified by the LO center frequency between 325 and 3800 MHz.

By running the openwifi project, X310 can send and receive Wi-Fi data through two antennas. The openwifi project is equipped with the CSI tool that can directly collect CSI readings. The sender and receiver are operating on the 2.412 GHz channel. The data rate is 200 packets per second. No unique design is required for data packets in Pa-Count, as we observe the CSI signal's amplitude fluctuation. The current 802.11 Wi-Fi standard stipulates that the AP needs to send ping packets to the connected STA every 0.1 seconds. The protocol's provisions ensure a long-term data transfer without interrupting ongoing data communications.

2) Signal Quality Enhancement: Considering that the Wi-Fi CSI signal caused by fidgeting is weak, we need to improve the signal quality by pre-processing operations, i.e., environmental interference elimination and enhancement of signal granularity.

Environmental Interference Elimination. As shown in Fig. 4(a), the environmental interference in a moving vehicle mostly comes from the vibration of the vehicle. The good news is that the frequency of these interference is much lower. We conduct several experiments on cars, buses and subways, and the frequency distribution from vehicle vibration is shown in Fig. 2. These environmental interference can be eliminated by a high-pass filter with a cutoff frequency of 20 Hz.

Enhancement of Signal Granularity. For further enhance the signals, we employ a Savitzky-Golay filter to improve the signals granularity. The purpose is to remove small random changes in the signal, leaving large changes due to activity. Savitzky-Golay filter (also known as least-square smoothing filter) fits successive subset of adjacent data points with a low degree polynomial by the method of linear least square [35]. After applying the filter, the raw signal is smoothed (see the red line in Fig. 3).

C. Fidgeting Detection

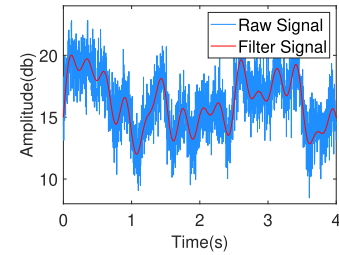In this subsection, we quantitatively calculate how human movement affects the signal amplitude through the Fresnel detection model. Then we conduct statistics and analyze the distribution function of passengers' fidgeting from the frequency and duration characteristics. Following that, we capture fidgeting motion by the signal amplitude fluctuation, and use a sliding window based on variance threshold for the detection of fidgeting event.

1) Fresnel Detection Model: Human activities affect the propagation of wireless signals. To specify, the activities of the human body will cause the diffraction of the signals, which is finally reflected in the signal fluctuations at the receiving end. Moreover, different activities will cause corresponding signal fluctuations, and the pattern of this fluctuation corresponds to the specific activity. [36] realized the identification and monitoring of activities through a diffraction-based sensing model in the Fresnel zone. It is accordingly adequate and robust to identify and monitor human activities by signal diffraction.

Motivated by this phenomenon, we elaborate how human activity causes diffraction and affects the wireless signals. Considering a free-space scenario, the transmitter antenna Tx and the receiver antenna Rx are set at two points of distance *2 d*. Tx transmits RF signals with a wavelength of λ. There is an ellipse (shown as Fig. 5) with Tx and Rx as focus. The ellipse zone is defined as

$$|TxP| + |RxP| - |TxRx| = \frac{\lambda}{2}, \qquad (1)$$

where P is a point on the ellipse [37]. There is a point *O* on the line connecting Tx and Rx and the distance is d_1 and d_2. Then the radius of this ellipse can be calculated as $r = \sqrt{\frac{\lambda d_1 d_2}{d_1 + d_2}}$ or $r = \sqrt{\frac{\lambda d}{2}}$ when $d_1 = d_2 = d$. The authors in [38] shows that between a pair of transceivers more than 70% of RF signals energy is transferred via the ellipse Zone. If a target moves into the ellipse, diffraction will become much stronger and dominates. Because the target blocks the primary energy pathway, the remaining energy needs to bypass the target. Therefore, the movements of the target within this ellipse may cause significant energy changes.

We focus on how signal propagation is affected when the target moves back and forth in the ellipse. Theoretical derivations are made in the horizontal plane of the two antennas, consequently we set the target as a circle and only consider the target movement along the vertical direction of the antenna connecting line. As shown in Fig. 5, the d_f is the distance from the target's front point to the ellipse's long axis. Similarly, d_b is the distance from the back point of the target to the long axis
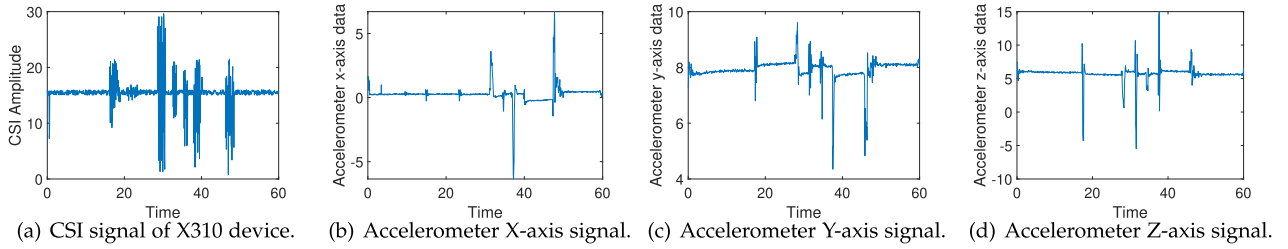
Fig. 4. (a) shows the fluctuation of CSI signal amplitude, (b), (c) and (d) show the accelerometer signal amplitude variation.

(a) CSI signal of X310 device. (b) Accelerometer X-axis signal. (c) Accelerometer Y-axis signal. (d) Accelerometer Z-axis signal.
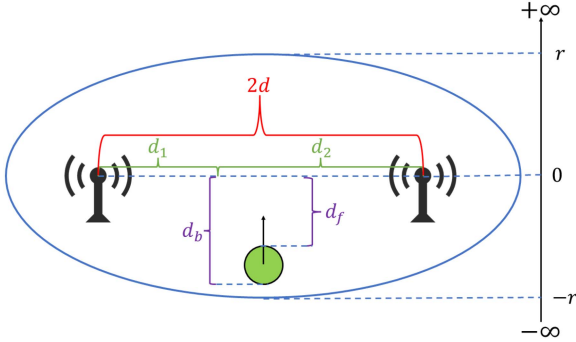

Fig. 5. Ellipse zone schematic diagram.

of the ellipse. We specify the direction of motion to facilitate subsequent calculations. All the variables are positive or negative depending on the direction. Then we can calculate

$$v_f = d_f \sqrt{\frac{2(d_1 + d_2)}{\lambda d_1 d_2}} = d_f \frac{\sqrt{2}}{r}, \qquad (2)$$

where v_f is diffraction parameter. Therefore, when the object position is still negative, the signal amplitude is the integral of the diffraction of the signal on the front side of the object to infinity, which can be expressed by

$$F(v_f) = \frac{1+j}{2} \int_{v_f}^{\infty} exp\left(\frac{-j\pi z^2}{2}\right) dz, \qquad (3)$$

where the $exp(\frac{-j\pi z^2}{2})$ is the phase shift for a diffraction path z. Integration to z from v_f to positive infinity accumulates all the signal paths that are diffracted from the front side of the target. Similarly, after the object crosses the line between the two antennas, the signal's amplitude is the integral of the signal diffracted from negative infinity to the back of the target. We integrate over z from negative infinity to v_b, so that accumulate the path diffracted from the back side of the target, which is given as follows

$$F(v_b) = \frac{1+j}{2} \int_{-\infty}^{v_b} exp\left(\frac{-j\pi z^2}{2}\right) dz. \qquad (4)$$

Above all, the derivation considers a special scene and then quantitatively obtains the fluctuation of signal amplitude caused by the diffraction of the moving target. The conclusion can be extended to a more general scenario and qualitatively prove that target movement causes fluctuation in signal amplitude.

2) Analysis of Fidgeting: In this subsection, we analyze passenger behavior and study the characteristics of signals caused by passenger fidgeting. First, we propose two basic concepts: silent period and fidgeting period. In a moving vehicle, most of the passengers have no physical movement other than breathing. It is difficult for passengers to remain completely still for a long time, instead, they unconsciously perform fidgeting including adjusting sitting posture, cross-legged, looking at mobile phones, scratching, stretching, coughing, etc. Most fidgeting are subconscious, in place, and subtle. When there is more than one passenger in the vehicle, the period in which all passengers have no movement other than breathing is called the silent period. As long as at least one passenger in the crowd is fidgeting, the period of the passenger crowd is called fidgeting period.

Frequency and Duration of Fidgeting. Generally, similar events will have an equal frequency and duration of fidgeting. But if the events are different, the frequency and duration of fidgeting may show a big difference because different events will have different levels of attraction. The attractiveness of different events, or in other words, the people's concentration at different events, may be one of the most important factors affecting the frequency and duration of fidgeting [24]. The famous 19th-century psychologist Francis Galton gave a public lecture in 1885 that invited an audience of 50 to fully simulate an actual speech without telling them about the experiment. Francis observed the fidgeting of this group of listeners based on the long-term observation. He concluded that the frequency of fidgeting for an individual while listening to the speech was once a minute [39]. Inspired by this experiment, we conduct a series of new observational experiments on different vehicles, and recorded the average frequency and duration distribution of fidgeting by using mobile phone cameras. The experimental results are shown in Fig. 6. The start time of fidgeting in three vehicles is 50–55 seconds, consequently the frequency distribution of fidgeting under the three vehicles is similar, and the duration time show the same distribution. The conclusion is that taking on different vehicles can be seen as similar events, and it follows similar distributions of fidgeting frequency and duration. In other words, individual passengers taking different vehicles present similar distribution of fidgeting frequency and duration.

The Effect of Crowding on Distribution. In the following, we explore the effect of crowding on fidgeting. The experiment is set up in a 5-seat car, and the data of passenger fidgeting frequency and duration are collected in two scenarios: there are only 3 passengers (there is only one passenger in the back, not crowded) and 5 passengers (there are 3 passengers in the back, crowded).
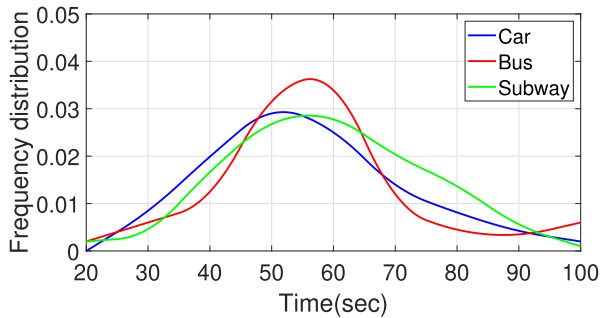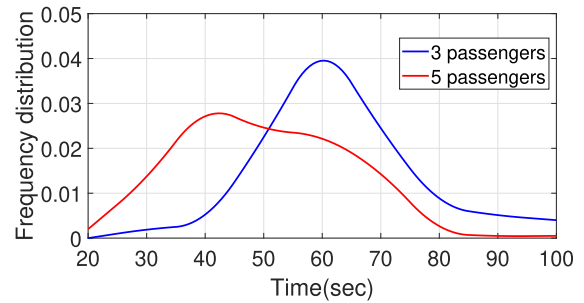
(a) Frequency distribution
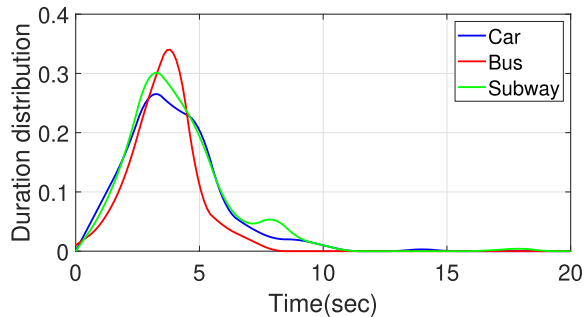
(b) Duration distribution

Fig. 6. The frequency and duration distribution in three different vehicles.

(a) Frequency distribution

(b) Duration distribution

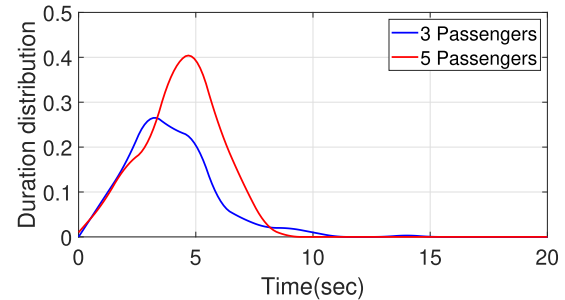Fig. 7. The frequency and duration distribution in different degree of crowdedness.

The experimental results are shown in Fig. 7. In crowded scenario, experiments show a higher frequency and longer duration of fidgeting. The reason is related to concentration, i.e., greater concentration in a spacious environment reduces the fidgeting. Besides, the narrow environment in the car will cause passengers' discomfort, which will lead to a higher frequency of fidgeting. Compared to the frequency distribution, the difference in the distribution of duration is not as obvious, because fidgeting movements have a similar duration, the duration is less affected by crowding.

3) Fidgeting Motion Capture: Recall the first paragraph of Section III-C2, we divide the status of a passenger in the vehicle into two categories. One is the fidgeting period. The other is the silent period. When a passenger is in the silent period, the only body movement is the slow sinusoidal breathing motion of the chest and abdomen. According to [40], the maximum normal breathing rate of adults is $f_{breath} = 0.3$ Hz. When a passenger is in the fidgeting period, the instantaneous speed of the body parts can increase significantly.

Chest movement caused by breathing is insignificant compared to the physical movements caused by fidget accordingly. As such, with a high probability, the received Wi-Fi CSI signals will have a higher frequency and amplitude than the one when only breathing. In addition, when a passenger is engaged in non-breathing in-place motion (e.g., fidgeting), the instantaneous speed of the body parts can increase significantly. On this basis, [41] attached accelerometers to the wrists of 20 subjects to analyze their motion while doing various tasks, one of which was sitting down and relaxing, and published the acceleration data in the PhysioNet database [42].

We study this dataset and calculate the speed of body motion during the relaxing periods from their published acceleration data. We find out that, during fidgeting, the speed of the body motion is larger than 0.01 m/s (which is the maximum body speed during breathing) 90% of the time. Furthermore, the speed of the body motion during fidgeting can take much larger values, e.g., five times the maximum body speed during breathing (or larger) for 80% of the time. It can even reach speeds as high as 3 m/s (i.e., 300 times larger). As such, with a high probability, the received Wi-Fi CSI magnitude or phase difference signal during a fidgeting will have a considerably higher frequency content than when only breathing. Thus, we can easily extract the fidgeting-related content by properly designing high-pass filter for the received Wi-Fi signal (phase difference or magnitude).

In fidgeting period, there is a noticeable fluctuation in the signal. Compared with the relatively flat signal in silent period, the amplitude is much higher. Based on this observation, we conduct experiments and the results are shown in Fig. 4. The experiment is done by a single experimenter, who shake head in 17 s, turn the body in 28 s, shake head again in 31 s, stretch in 34 s, adjust the glasses in 37 s and move the body against the backrest in 46 s. Fig. 4(a) shows the CSI amplitude signal captured by the X310 device, Fig. 4(b), (c) and (d) shows the signals in the x, y, and z axes of the accelerometer placed on the experimenter's chest. It can be clearly seen that the CSI amplitude through Wi-Fi communication in Fig. 4(a) has apparent fluctuations at 17 s, 28 s, 31 s, 34 s, 37 s and 46 s. At the same time, the signals in the x, y, and z axes of the accelerometer have a similar trend. And the signal in the z-axis is most identical to the difference in the CSI amplitude shown as Fig. 4(b), (c), and (d), indicating that the accelerometer z-axis is the main axis in the fidgeting
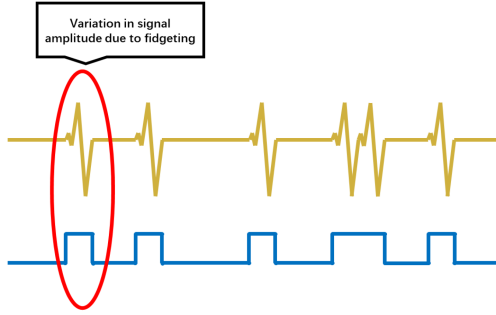
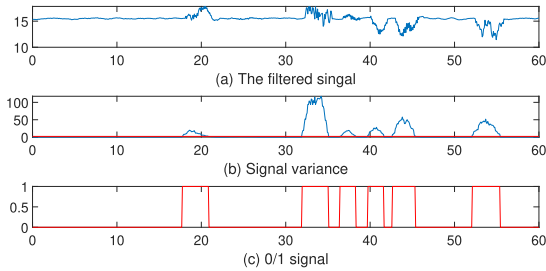Fig. 8.   Fidgeting and silent signal to 0/1 signal.

Fig. 9.   Event detection: (a) shows the filter signal amplitudes, (b) shows the calculated signal variance. The horizontal solid red line is the variance threshold. The starting and ending points of an activity can be clearly identified. (c) shows the 0/1 high and low level signal.

of the volunteer. Most importantly, we can see that fidgeting can cause significant amplitude fluctuations compared to the relatively stable amplitude of the CSI signal measured only by breathing during the silent period.

4) Fidgeting Event Detection: After capturing fidgeting motion, we detect the fidgeting event through sliding window based on variance threshold. In particular, we abstract the collected fluctuating and stationary signals into 0/1 level analog signals. As shown in the Fig. 8, the peak is regarded as high level '1' which represents that passenger crowd is in fidgeting period and the steady wave is regarded as low level '0' which means passenger crowd is in silent period.

For extracting response fragments, Pa-Count adopts a variance threshold-based sliding window method to determine boundary points. As illustrated in Fig. 4(a), whether the passenger crowd is in fidgeting period determines the amplitude of CSI signal, we use the variance of CSI signal amplitude to detect fidgeting events. According to the signal variance shown in Fig. 9(b), it can be observed that when the passenger crowd is in the fidgeting period, the variance is higher than 20, in contrast, the variance in the silent period closes to 0. Empirically, we set the variance threshold to 1 and use a sliding window of 0.2 seconds to estimate the magnitude of the variance. Fig. 9(c) shows the 0/1 signal, '0' indicates that the passenger crowd is in the silent period, and '1' indicates the occurrence of fidgeting among passengers.

D. Passenger Counting

In this subsection, we establish the relationship between passenger fidgeting and numbers. To that end, we utilize the power
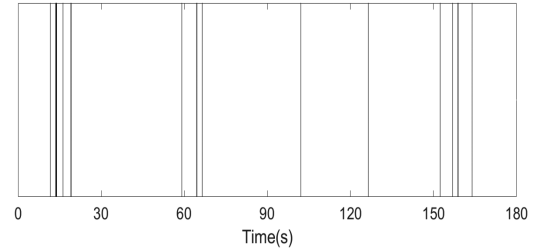

Fig. 10.   Experimentally measured time of fidgeting.

law with exponential cutoff distribution to estimate the passengers fidgeting. Based on the distribution function and queuing theory, we establish a counting model using the Maximum A Posteriori (MAP) estimation to count the passenger numbers.

1) Distribution for Describing Passengers Fidgeting: In order to establish the relationship between passenger fidgeting and the number of passengers, we first figure out the fidgeting distribution function. [24] used the Poisson distribution to describe human fidgeting by comparing fidgeting and silent periods to the busy and idle periods in the M/G/∞ queuing theory. Nevertheless, this method performs poor in the vehicle scenarios. To cope with this problem, we develop the Power law with exponential cutoff distribution to estimate the passengers fidgeting. In the function image drawn by measured data (especially in the distribution of interval time), the tail of the function has obvious heavy tail phenomenon, which is not similar to Poisson distribution. Compared with the Poisson distribution, the heavy tail phenomenon in the Power law with exponential cutoff distribution decays slowly and drags a long tail, making the probability of large observation values appear much higher than the prediction based on the Poisson distribution. This phenomenon reflects in the distribution law of time interval, namely the "paroxysmal" feature. According to [43], paroxysmal can be quantitatively expressed as:

$$B = \frac{\sigma_\tau - m_t}{\sigma_\tau + m_t}, \tag{5}$$

where σ_τ and m_t represent the standard deviation and mean value of the distribution $p(\tau)$, respectively. The value of B is between -1 and 1. For the Poisson distribution, the mean and standard deviation are equal, hence the paroxysmal is exactly 0. The experimental data shows that the distribution standard deviation of passengers fidgeting on the vehicle is greater than the mean, and B is close to 1. Experimental data confirms the "paroxysmal" as shown in Fig. 10. Note that there are long silent periods and intense fidgeting periods or a long fidgeting period is followed. Notably, passengers' fidgeting distribution does not completely follow the Poisson distribution and has large paroxysmal. The reasons are as follows. First, passengers fidgeting in the vehicle will be affected by the surrounding environment, which is different from the static scene; secondly, the more closed environment in the vehicle leads to each passenger fidgeting is not independent. According to [44], this phenomenon indicates that the tail of the distribution obeys a power law. Inspired by this, we use the function with power law with exponential cutoff distribution to estimate passenger fidgeting.
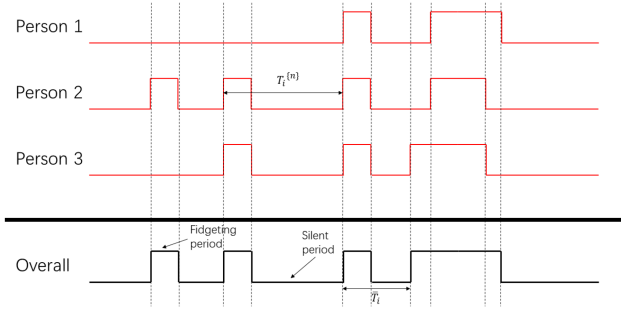
Fig. 11. Timeline of 3 people in the vehicle.

2) Fidgeting Model: We leverage the queue theory to calculate the number of passengers. Based on [45], we can regard the calculation of passengers by fidgeting as the problem of calculating the number of servers occupied by customers in the case of infinite servers. The time distribution of customer arrival to the server satisfies the power law with exponential cutoff distribution. In the following, we define several variables based on the queuing theory. Let $t_i^{\{n\}}$ denote the start of the i-th fidget of the n-th passenger and $d_i^{\{n\}}$ denote the time duration of the i-th fidget of the n-th passenger Table 1. Thus, $T_i^{\{n\}} = t_i^{\{n\}} - t_{i+1}^{\{n\}}$ is the i-th interval time of the n-th passenger. $T_i^{\{n\}}$ follows an exponential distribution:

$$p\left(T_i^{\{n\}} = t\right) = \lambda^{\{n\}} e^{-\lambda^{\{n\}} t}, \tag{6}$$

where $\lambda^{\{n\}}$ denotes the n-th passenger's average incidence of fidgeting per unit time. Let $\overline{T}_i$ (shown as Fig. 11) denote the i-th interval time of all passengers in the vehicle. Different from [45], the distribution of $\overline{T}_i$ can no longer be the superposition of $T_i^{\{n\}}$, but follows the power law with exponential cutoff distribution:

$$p(\overline{T}_i = t) = \left(\sum_{n=1}^{N} \lambda^{\{n\}}\right) e^{-t\left(\sum_{n=1}^{N} \lambda^{\{n\}}\right)} t^{-\sum_{n=1}^{N} \lambda^{\{n\}}}. \tag{7}$$

Accordingly, the distribution of interval time can be derived by Eq. (8)

$$p_S(s|N) = \overline{\lambda} N e^{s\overline{\lambda} N} s^{-\overline{\lambda} N}, \tag{8}$$

where the $\overline{\lambda}$ is passengers' average incidence of fidgeting per unit time. Let

$$C(t) := 1 - e^{-\overline{\lambda} \int_0^t (1 - H(x)) dx}, \tag{9}$$

$$c(t) := C'(t) = \overline{\lambda}(1 - H(t))(1 - C(t)), \tag{10}$$

where $H(.)$ represents the cumulative distribution function with its probability distribution function $h(.)$. According to [46] [47], $h(.)$ can be expressed as

$$h_d(t) = \sum_{k=0}^{[t/\overline{b}]-1} (-1)^k (k!)^{-1} \left(\overline{\lambda} e^{-\overline{b}\overline{\lambda}}\right) \{(t - \overline{b}(k+1))^k - e^{-\overline{b}\overline{\lambda}}(t - \overline{b}(k+2))^k\}, \tag{11}$$

where $\overline{b}$ is the average duration times of a passenger and $[t/\overline{b}]$ denotes the largest integer $\leqslant t/\overline{b}$. Based on the [45], the distribution of fidgeting period can be derived by Eq. (12):

$$p_F(f|N) = \frac{d}{df}\left(1 - \overline{\lambda}^{-1} N \sum_{i=1}^{\infty} \right.$$
$$\left. \times \left[\left(1 - \int_0^f h(x)dx\right)(1 - C(f))\right]^{*i}\right). \tag{12}$$

3) Calculation of the Number: Based on 0/1 signal extracted from CSI signal, "1" signals are successively denoted as $f_1, f_2, \ldots, f_{N_f}$, and "0" signals are denoted as $s_1, s_2, \ldots, s_{N_s}$. According to the analysis in [48], the number of passengers N can be MAP estimated as

$$N(t), \overline{\lambda} = \arg\max_{N, \overline{\lambda}} p\left(N, \overline{\lambda} \mid g_1, \ldots, g_{N_f}, s_1, \ldots, s_{N_s}\right)$$
$$= \arg\max_{N, \overline{\lambda}} \frac{p(N, \overline{\lambda})p(g_1, \ldots, g_{N_f}, s_1, \ldots, s_{N_s} \mid N, \overline{\lambda})}{p(g_1, \ldots, g_{N_f}, s_1, \ldots, s_{N_s})}, \tag{13}$$

and $p(N, \overline{\lambda} \mid f_1, \ldots, f_{N_f}, s_1, \ldots, s_{N_s})$ is independent of N. It can be written as

$$N(t), \overline{\lambda} = \arg\max_{N, \overline{\lambda}} p(N, \overline{\lambda})p\left(f_1, \ldots, f_{N_f}, s_1, \ldots, s_{N_s} \mid N, \overline{\lambda}\right)$$
$$= \arg\max_{N, \overline{\lambda}} p\left(f_1, \ldots, f_{N_f}, s_1, \ldots, s_{N_s} \mid N, \overline{\lambda}\right) p(N)p(\overline{\lambda}), \tag{14}$$

where $p(N)$ is taken as uniform, because we do not assume any prior knowledge on the number of passengers N. Therefore, the number of passengers N can be derived as

$$N(t), \overline{\lambda} = \arg\max_{N, \overline{\lambda}} p(\overline{\lambda}) \prod_{i=1}^{N_f(t)} p_F\left(f_i \mid N, \overline{\lambda}\right) \prod_{j=1}^{N_s(t)} p_S\left(s_j \mid N, \overline{\lambda}\right). \tag{15}$$

Taking the logarithm does not affect the optimal value, N can be finally expressed as

$$N(t), \overline{\lambda} = \arg\max_{N, \overline{\lambda}} \ln p(\overline{\lambda}) + \sum_{i=1}^{N_S} \ln p_S\left(s_i \mid N, \overline{\lambda}\right)$$
$$+ \sum_{j=1}^{N_f} \ln p_F\left(f_j \mid N, \overline{\lambda}\right), \tag{16}$$

where $p(.)$ denotes the probability of the argument. Among them, $p_F(f_j \mid N, \overline{\lambda})$ and $p_S(s_j \mid N, \overline{\lambda})$ are calculated in Section III-D2. To obtain the real-time number of passengers, we need to achieve the prior distribution of all passengers' average incidence of fidgeting per unit time $p(\overline{\lambda})$ and the average duration times of a passenger $\overline{b}$ through experiments.

IV. SYSTEM IMPLEMENTATION

Hardware Implementations. As shown in Fig. 12, the core component of Pa-Count is a compacet and low-cost X310 device. The device is equipped with openwifi firmware which is a software-defined radio (SDR) design based on zynq+AD9361, which is an implementation of the IEEE 802.11/Wi-Fi protocol.
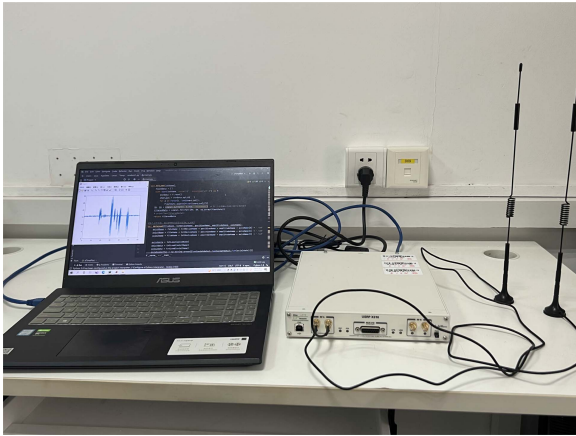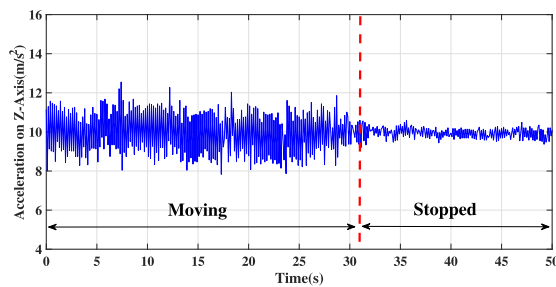
Fig. 12.   System implementation of Pa-Count.

Fig. 13.   The average amplitude of signals and reads from the accelerator's z-axis when Vehicle Driving and Stopped.

Data is sent and received through two antennas placed in the front left and rear right of the vehicles. The fidgeting detection module and counting model are both implemented using Python 3.7. All code will be executed on a laptop computer (GTX 1650 graphincs card and I7-7700).

Initiation and Termination of Pa-Count. Pa-Count should be suspended when the vehicle is in a stopped state and be initiated when the vehicle is moving smoothly. In the conditions that every vehicles start or stop will be possibly accompanied by the changes in passenger numbers. Pa-Count determines whether the vehicle is moving by the vibration amplitude of the acceleration sensor. There will be a certain amount of shaking when the vehicle is moving, and these shaking will be directly reflected in the vertical direction, as shown in Fig. 13. Based on the fluctuations, the system will start or pause.

Ground Truth. We set up a separate mobile phone at the back seat of the vehicle and the connection of the subway as a record, and we can use the camera function of this mobile phone to monitor the road and track conditions. The phone can be held by hand and is also equipped with a tripod with adjustable height angle and position. The height of the phone is set at the same level as the two antennas.

V. EVALUATION

In this section, we comprehensively evaluate the passenger counting performance of Pa-Count by varying the parameters under different conditions.

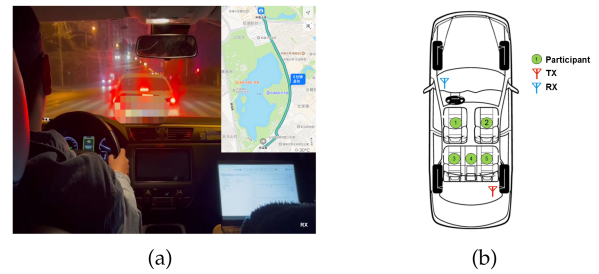(a)   (b)

Fig. 14.   Car experiment scene: (a) Passenger counting test in a 5-seat SUV. The total length of the test section is 1.7 kilometers, and the average test speed is 35 km/h. (b) Seating configuration: The five positions in the car (including the driver's seat) are numbered 1-5 in sequence, and are divided into 8 seat configurations according to the number of people and usage habits.

A. Experiment Setup

In the Pa-Count, the Wi-Fi CSI signal is sent every 1 s. At the receiving end, the signal is sampled at a sampling rate of 2.4 GHz. The layout of the antenna is shown in Fig. 12.

We recruit a total of 12 volunteers (7 men and 5 women) to systematically evaluate the performance of Pa-count. The volunteers' heights range from 1.60 m to 1.84 m, and their ages range from 20 to 50. We first evaluate the effectiveness and accuracy of the Pa-Count method. Then we conduct experiments in two types of vehicles, i.e., the private car and the coach in subway, to evaluate the overall performance. Each volunteer participates in at least two experiments, and each experiment lasts around two hours.

Setup in a Car. We conduct 16 experiments counting passengers in a car. The number of volunteers participating in the experiments is 2 to 5 passengers. The experimental vehicle is a 5-seat SUV, and the driving environment is a urban road with several vehicles. The average speed during the experiment is 30 km/h. Fig. 14(a) shows the experiment scenario. The transmitting antenna is placed on the left front side of the car, and the receiving antenna is placed on the right rear side. The 5 positions of the SUV are numbered 1 to 5 respectively, as shown in the Fig. 14(b). As the absolute difference between the estimated and true number of passengers ($e = |\hat{N} - N_{true}|$), the accuracy can be expressed as $p(e \leq 1)$. In the car, $p(e \leq 1)$ indicates the proportion of 0 error counting.

Setup on the Subway. In the selected carriage of subway, we conduct 30 experiments for passenger counting. As shown in Fig. 15(a), the experimental scene is in Changsha Metro Line 3, and the test section is from Yangguang Station to Shantang Station. We carry out the experiments during 10:00 pm to 11:00 pm. We choose an empty carriage of subway with no passengers except volunteers for the experiments. As shown in Fig. 15(b), we divide the carriage into three areas, which are the left seating area (Left), the right seating area (Right), and the standing area (Stand). The transmitting and receiving antennas are arranged respectively in the front right and rear left of the carriage. Considering the piratical situation, a maximum of 6 volunteers can be arranged in the seating area, and a maximum of 6 volunteers are arranged in the standing area. In the subway, $p(e \leq 1)$ indicates the proportion of 0 or 1 error counting.
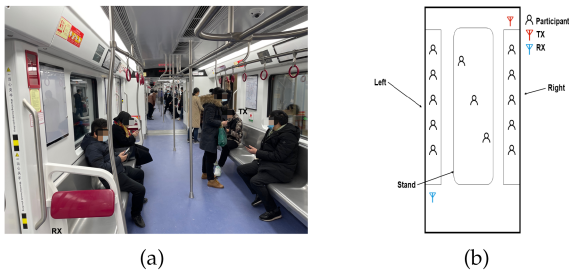
(a) (b)

Fig. 15. Subway experiment scene: (a) The environment of the subway test sample experiments: Changsha Metro Line 3 from Yangguang Station to Shantang Station. (b) Divided into left area, right area, stand area. Left and right area can accommodate up to 6 passengers and stand area can accommodate up to 6 passengers.
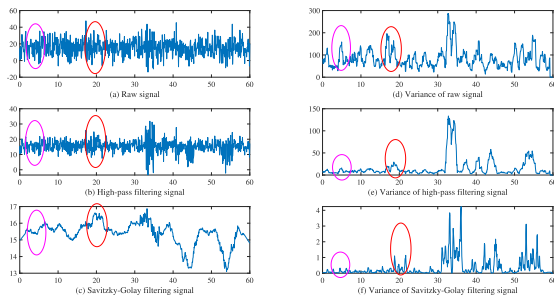

Fig. 16. Evaluation of filter in car scenario.

Fig. 17. Evaluation of filter in subway scenario.

Fig. 18. The power law with exponential cutoff distribution and the experimental probability.

B. Evaluation by the Pa-Count Method

1) Performance of Interference Elimination and Signal Enhancement: The experimental scene is a moving car with 4 passengers on bumpy road and a moving subway with 6 passengers, we show a 60-second signal clip. As shown in Fig. 16, the X-axis represents time, and the Y-axis represents amplitude in (a), (b), (c) and variance in (d), (e) and (f). Signal types include raw signal without filtering (e.g., Fig. 16(a)), high-pass filtering signal (e.g., Fig. 16(b)), and Savitzky-Golay filtering signal (e.g., Fig. 16(c)). We show a silent period circled by purple and a fidgeting period circled by red. In Fig. 16(a), there is no difference between silent period and fidgeting period in the raw signal. The signal filtered by high-pass filter to eliminate the environmental interference is shown in Fig. 16(b). Because low frequency environment interference is filtered out, the distinguishable of fidgeting period is improved. But there is still a high degree of similarity between silent period and fidgeting period. After Savitzky-Golay filtering, there is a clear distinction between the fidgeting period and the silent period in the signal shown in Fig. 16(c). Then we obtain a more obvious effect by sliding window by variance. Fig. 16(d), (e) and (f) plot the variance of 3 signals, in Fig. 16(d) and Fig. 16(e) the purple and red circled signals both have a fluctuation which may be judged by the system to be fidgeting period. In Fig. 16 (c) it's easy to distinguish between silent period and fidgeting period by a threshold of 1. The evaluation results on the subway is shown in Fig. 17 with a 8 passengers experiment. As in the car, silent period and fidgeting period can be easily distinguished by the variance of the 1-threshold through the filter combination. We conduct 25 experiments separately on
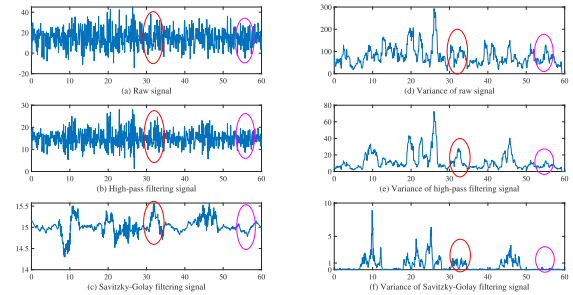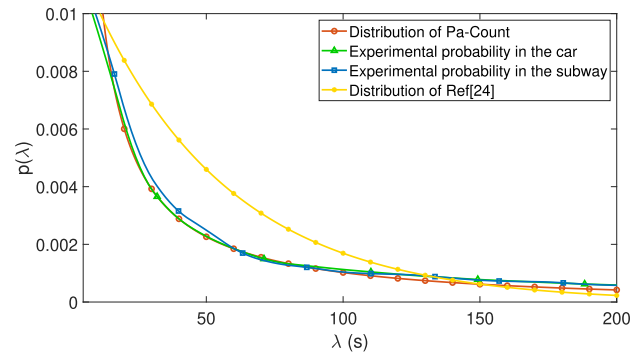
flat roads, bumpy roads and subways, including 4 passengers in a car and 8 passengers in a subway shown as Figs. 14 and 15. The performance is shown as follows, the accuracy reduces from 92.4% to 81.8% on flat roads, and even from 88.75% to 72.9% on bumpy roads, and in the subway drops from 90.4% to 82.2%.

2) Validity of the Counting Model: Recalling Eq. (16), the real number of passengers is the x-coordinate N when the Number Dependence Function is maximized. We rewrite the Number Dependence Function as:

$$f(N) = \ln p(\bar{\lambda}) + \sum_{i=1}^{N_S} \ln p_S(s_i \mid N, \bar{\lambda}) + \sum_{j=1}^{N_f} \ln p_F(f_j \mid N, \bar{\lambda}).$$

We can obtain *f(N)* through p_F and p_S obtained by signals, and $p(\bar{\lambda})$ from the priori experiments.

In the following, we evaluate the rationality of the model, Probability Distribution Function $p(\lambda)$, and distribution of fidgeting duration $p_F(f)$. *Effectiveness of the distribution of interval time.* In Section III-D2, we build the fidgeting model based on the fact that we model passenger fidgeting based on statistics of human behavior. In this section, we evaluate the rationality of this model. We collect the interval time λ of five passengers fidgeting on the subway and the car. Then we put all the data in one pool to achieve an average probability, and we draw Fig. 18 to show its similarity. It's very distinct from the exponential distribution. At the same time, we calculate the Kullback-Leibler divergence of the two functions to quantitatively judge their similarity. The KLD between the model and the experimental data is 0.157 and 0.145. Hence, the power law with exponential cutoff
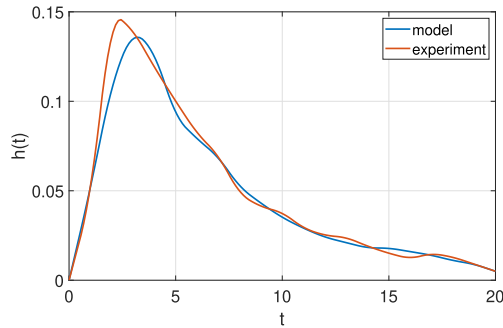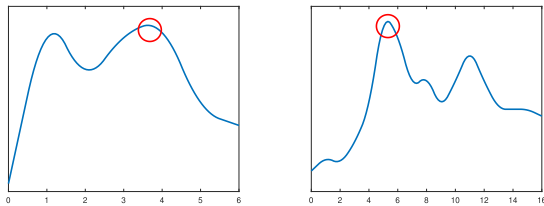
Fig. 19. The fidgeting duration function.

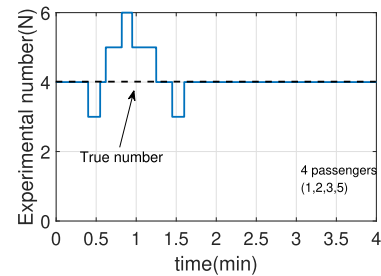Fig. 20. The argmax function implementation.

Fig. 21. Counting results: as a function of time, for an experiment with 4 passengers in a (driver's seat:1, right front seat:2, left rear seat:3, right rear seat:5) configuration.

TABLE II
COUNTING RESULTS IN 16 EXPERIMENTS

True number	Seating config	Pa's error	Ref [24]'s error
2	(1,2)	0	0
2	(1,2)	0	0
2	(1,3)	0	0
2	(1,3)	0	1
2	(1,5)	0	0
2	(1,5)	0	0
3	(1,2,5)	0	0
3	(1,2,5)	0	0
3	(1,2,3)	0	0
3	(1,2,3)	0	0
3	(1,3,5)	0	1
3	(1,3,5)	0	0
4	(1,2,3,5)	1	0
4	(1,2,3,5)	0	0
5	(1,2,3,4,5)	0	2
5	(1,2,3,4,5)	0	0

distribution can accurately describe the fidgeting of passengers in the vehicle.

Effectiveness of Fidgeting Duration Function. In Section II-I-D2, we propose the fidgeting duration function $H(.)$ to derive the fidgeting period model. In this section, we compare the experimental data with the ideal model to verify the model's validity. As shown in Fig. 19, the curve is similar. Then we carry out the least square fitting between power law with exponential cutoff distribution and the data we obtained in the experiments. The coefficient of determination R^2 is 0.956. Therefore, the function is valid in the counting model.

Implementation of Number Dependence Function. Based on the above analysis, we can calculate the Number Dependence Function *f(N)*, and we show it in Fig. 20. The X-axis is the number of passengers N, and the Y-axis is the value of the *f(N)*. We extract signal data from the experiments in the car and vehicle, respectively. We observe that x-coordinate value corresponds to the maximum value of the function, which indeed indicates the real number of passengers (the observation step is replaced by the *argmax* function in the model). It proves the validity of counting model that the number of passengers reflected in the figure is consistent with the real number. Next, we will further evaluate Pa-Count in two real scenarios.

C. Overall Performance

1) Counting in Different Environments: In Section V-A, we propose the experimental setup in a car and on the subway. In this section we will evaluate the performance of Pa-Count in real scene in a car and on the subway.

Counting in a Car. We set up 8 groups of experiments, each group consists of two experiments with the same seat distribution, and each experiment lasts 5 minutes. One of the experimental results of 3 passengers (passenger positions 1, 2, 5) is shown in Fig. 21. Note that the data will fluctuate to a

certain extent in the first three minutes, the reason is that the initial amount of data is too small to calculate the real number of passengers. After 1.5 minutes, the data converges to the real number of passengers. Table II shows that Pa-Count can maintain an accuracy of 93.75%.

Counting in a Subway. Fig. 23 shows the change of the number of passengers in one of the experiments. During the experiment, there are certain fluctuations at the beginning, and it converges to the real number of passengers within two and a half minutes. Based on the results in Table III, Pa-Count can achieve 92.6% accuracy when the number is less than 16.

2) Impact of Accuracy: Impact of the distance between Tx and Rx antennas. To meet the requirements of the Fresnel zone, the antenna positions can only be placed at the opposite corner of the vehicle. We move the antennas distance in steps of 10 cm along the diagonal of the experimental space (the step length of the receiving antenna and the transmitting antenna is 5 cm each). There is a slight increase in detection accuracy with the decrease of distance due to reduced reflection signal-to-noise ratio, but these accuracy shifts are small. Due to the limitation of the compartment space, the antennas distance in the subway has little effect on the measurement accuracy. At the same time, because the car compartment space is narrower, the position where the antenna can move is extremely limited. As a result, the distance has little impact to the performance of passenger counting.
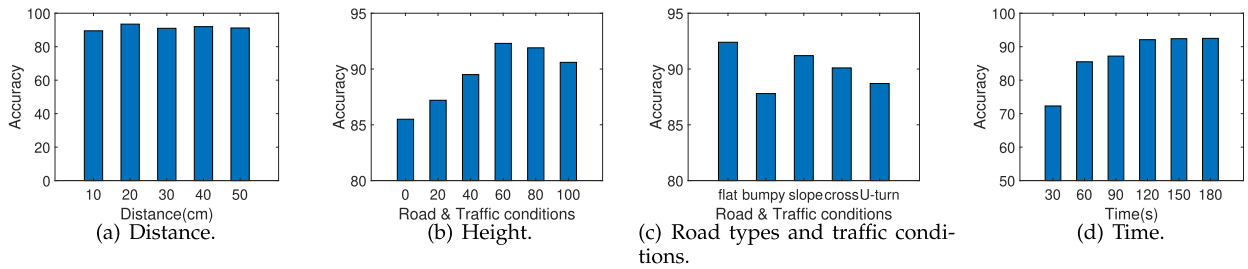
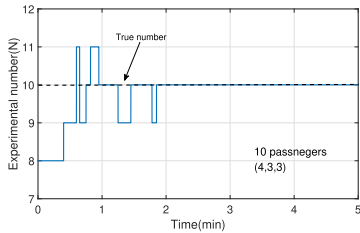Fig. 22. Differences in accuracy under different influencing factors.

Fig. 23. Counting results: as a function of time, for an experiment with 10 passengers in a (left area:4, right area:3, stand area:3) configuration.

TABLE III
FINAL COUNTING RESULTS FOR ALL THE 30 EXPERIMENTS CONDUCTED

True number	Seating config	Pa's error	Ref [24]'s error
2	(1,1,0)	0	0
2	(2,0,0)	0	0
4	(2,2,0)	0	0
4	(3,1,0)	0	0
6	(3,3,0)	0	0
6	(4,2,0)	1	1
8	(4,4,0)	0	0
8	(4,3,1)	0	0
8	(3,3,2)	0	2
10	(5,5,0)	0	0
10	(5,4,1)	0	0
10	(4,4,2)	1	0
10	(4,3,3)	0	0
11	(5,5,1)	2	0
11	(5,4,2)	0	1
11	(4,4,3)	1	0
11	(4,3,4)	0	1
12	(5,5,2)	0	2
12	(5,4,3)	1	0
12	(4,4,4)	2	3
13	(5,5,3)	0	1
13	(5,4,4)	0	1
14	(5,5,4)	1	3
14	(5,4,5)	0	0
15	(5,5,5)	0	1
15	(5,6,4)	1	2
15	(6,6,3)	0	0
16	(5,5,5)	1	1
16	(5,6,4)	2	3
16	(6,6,3)	2	2

TABLE IV
ACCURACY COMPARED WITH REF [24]

	Pa-Count	Ref [24]
Car	93.8%	81.3%
Subway	92.6%	85%

Impact of Antenna Height. To explore the effect of height, the antennas are placed from 0 to 100 cm height in 20 cm steps. We observe the best measurement accuracy at antenna heights of 60 to 80 cm, since human fidgets are mostly torso movements, and the height of 60 to 80 cm coincides with the height of the torso motion plane. When the height is too low or too high, because the impact of the height difference, the signal transmission power is limited. In this case, it is not easy for the Wi-Fi signals to reach the fidgeting position, resulting in a decrease in the perception performance.

Impact of Road Types. In order to investigate the robustness of Pa-Count on the road surface, we collect data on different road types (e.g., flat road, bumpy road, uphill section, downhill section, crossroads, and U-turns). The results are shown in Fig. 22. We observe that the vehicle on the flat road has the highest counting accuracy, and the bumpy road has a greater impact on the counting results.

Impact of the Detection Time. In the experiments, we find out that the Pa-Count has a large data fluctuation within 1.5 minutes after starting the signal detection and counting, the reason is too little time leads to great uncertainty in the distribution of passengers fidgeting. Consequently, the reaction time only occurs when Pa-Count is turned on, after which Pa-Count collects enough data to count in real time.

VI. CONCLUSION

In this paper, we have developed a passenger counting method in vehicles, the so-called Pa-Count, and then implement a passenger counting platform using Wi-Fi CSI signal on a X310 device. Through theoretical and experimental analysis, we eliminate the environmental interference of the moving vehicle and enhance the signal granularity through the combined filter for fidgeting detection. We propose a power law with exponential cutoff distribution of passenger fidgeting in a vehicle and verify its validity. Based on this distribution, we build a counting model to calculate the number of passengers in real time. Experimental results demonstrate the effectiveness of our system with over 92% accuracy in the vehicle scenario. We believe that the proposed counting approach can be applied to improve the performance of other sensing applications involving human behavior estimation Table 4.

Limitation and Future Work. This paper introduces a method to detect the number of people in vehicle using Wi-Fi CSI signal, but it has limitations. Since Pa-Count uses the passenger fidget

duty cycle to estimate the number of people, the first limitation is the maximum number of passengers. As part of future work, one can then utilize more resources, e.g., more antennas, for counting over larger areas that contain more passengers. The second limitation is measurement error when the vehicle shakes violently. In the future, we will devote effort in achieving continuous detection to extract the waveform of the acceleration sensor, and then use the waveform of the acceleration sensor at the receiving end to remove the influence.

REFERENCES

[1] American Public Transportation Association, "Public transportation facts," 2021. [Online]. Available: https://www.apta.com/news-publications/public-transportation-facts/

[2] Office of the Beijing Tianjin Hebei Collaborative Development Statistical Monitoring and Coordination Leading Group, "The regional development index for the coordinated development of Beijing Tianjin Hebei region continues to improve," 2021. [Online]. Available: http://www.stats.gov.cn/sj/zxfb/202302/t20230203_1901694.html

[3] "Maps & figures on the trans-European transport network (TEN-T)," 2023. [Online]. Available: https://ec.europa.eu/transport/infrastructure/tentec/tentec-portal/site/index_en.htm

[4] Z. Xiao et al., "Understanding private car aggregation effect via spatio-temporal analysis of trajectory data," *IEEE Trans. Cybern.*, vol. 53, no. 4, pp. 2346–2357, Apr. 2023.

[5] Z. Xiao et al., "On extracting regular travel behavior of private cars based on trajectory data analysis," *IEEE Trans. Veh. Technol*, vol. 69, no. 12, pp. 14 537–14 549, Dec. 2020.

[6] A. Lugo, N. Aquino, M. González, L. Cernuzzi, and R. Chenú-Abente, "Ucarpooling: Decongesting traffic through carpooling using automatic pairings," in *Proc. IEEE 46th Latin Amer. Comput. Conf.*, 2020, pp. 358–366.

[7] S. Amin, P. Jaillet, and M. Wu, "Efficient carpooling and toll pricing for autonomous transportation," 2021, *arXiv:2102.09132*.

[8] W. Cui, W. Dong, X. Sun, K. Feng, and J. Zhang, "A global dynamic capacity risk assessment and prediction method of regional rail transit network based on passenger flow monitoring," in *Proc. 13th Int. Conf. Comput. Model. Simul.*, 2021, pp. 95–103.

[9] Z. Li, Y. Wang, and Q. Chen, "Real-time monitoring of intercity passenger flows based on big data: A decision support tool for urban sustainability," *Int. J. Strategic Decis. Sci.*, vol. 8, no. 4, pp. 120–128, 2017.

[10] C. Chen et al., "TR-BREATH: Time-reversal breathing rate estimation and detection," *IEEE Trans. Biomed. Eng.*, vol. 65, no. 3, pp. 489–501, Mar. 2018.

[11] F. Wang, F. Zhang, C. Wu, B. Wang, and K. Liu, "Respiration tracking for people counting and recognition," *IEEE Internet Things J.*, vol. 7, no. 6, pp. 5233–5245, Jun. 2020.

[12] H. Jiang, J. Hu, D. Liu, J. Xiong, and M. Cai, "DriverSonar: Fine-grained dangerous driving detection using active sonar," *Proc. ACM Interactive Mobile Wearable Ubiquitous Technol.*, vol. 5, no. 3, pp. 1–22, 2021.

[13] J. Filipic, M. Biagini, I. Mas, C. D. Pose, and D. R. Parisi, "People counting using visible and infrared images," *Neurocomputing*, vol. 450, pp. 25–32, 2021.

[14] S. Zhang, Y. Wu, C. Men, and X. Li, "Tiny YOLO optimization oriented bus passenger object detection," *Chin. J. Electron.*, vol. 29, no. 1, pp. 132–138, 2020.

[15] W. Liu, X. Du, Q. Geng, J. Li, H. Li, and L. Liu, "Metro passenger flow statistics based on YOLOv3," in *Proc. IOP Conf. Ser. Mater. Sci. Eng.*, vol. 688, no. 4. IOP Publishing, 2019, Art. no. 044025.

[16] J.-H. Choi, J.-E. Kim, and K.-T. Kim, "People counting using IR-UWB radar sensor in a wide area," *IEEE Internet Things J.*, vol. 8, no. 7, pp. 5806–5821, Apr. 2021.

[17] T. Zheng, Z. Chen, S. Ding, and J. Luo, "Enhancing RF sensing with deep learning: A layered approach," *IEEE Commun. Mag.*, vol. 59, no. 2, pp. 70–76, Feb. 2021.

[18] S. Depatla, A. Muralidharan, and Y. Mostofi, "Occupancy estimation using only WiFi power measurements," *IEEE J. Sel. Areas Commun.*, vol. 33, no. 7, pp. 1381–1393, Jul. 2015.

[19] M. Nakatsuka, H. Iwatani, and J. Katto, "A study on passive crowd density estimation using wireless sensors," in *Proc. 4th Intl. Conf. Mobile Comput. Ubiquitous Netw.*, Citeseer, 2008, pp. 1–6.

[20] W. Xi et al., "Electronic frog eye: Counting crowd using WiFi," in *Proc. IEEE Conf. Comput. Commun.*, 2014, pp. 361–369.

[21] S. Di Domenico, G. Pecoraro, E. Cianca, and M. De Sanctis, "Trained-once device-free crowd counting and occupancy estimation using WiFi: A doppler spectrum based approach," in *Proc. IEEE 12th Int. Conf. Wirel. Mobile Comput. Netw. Commun.*, 2016, pp. 1–8.

[22] F. Xiao, Z. Guo, Y. Ni, X. Xie, S. Maharjan, and Y. Zhang, "Artificial intelligence empowered mobile sensing for human flow detection," *IEEE Netw.*, vol. 33, no. 1, pp. 78–83, Jan./Feb. 2019.

[23] Y. Yang, J. Cao, X. Liu, and K. Xing, "Multi-person sleeping respiration monitoring with cots wifi devices," in *Proc. IEEE 15th Int. Conf. Mobile Ad Hoc Sensor Syst.*, 2018, pp. 37–45.

[24] B. Korany and Y. Mostofi, "Counting a stationary crowd using off-the-shelf WiFi," in *Proc. 19th Annu. Int. Conf. Mobile Syst. Appl. Serv.*, 2021, pp. 202–214.

[25] D. Morales, I. Agudo, and J. Lopez, "Real-time crowd counting based on wearable ephemeral IDs," in *Proc. 19th Int. Conf. Secur. Cryptography - SECRYPT*, 2022, pp. 249–260, doi: 10.5220/0011327200003283.

[26] T. Amesaka, H. Watanabe, M. Sugimoto, and B. Shizuki, "Gesture recognition method using acoustic sensing on usual garment," *Proc. ACM Interactive Mobile Wearable Ubiquitous Technol.*, vol. 6, no. 2, pp. 1–27, 2022.

[27] C. Stauffer and W. E. L. Grimson, "Adaptive background mixture models for real-time tracking," in *Proc. IEEE Comput. Soc. Conf. Comput. Vis. Pattern Recognit.*, 1999, pp. 246–252.

[28] D. Gavrila and J. Giebel, "Virtual sample generation for template-based shape matching," in *Proc. IEEE Comput. Soc. Conf. Comput. Vis. Pattern Recognit.*, 2001, pp. I–I.

[29] P. Soviany and R. T. Ionescu, "Optimizing the trade-off between single-stage and two-stage deep object detectors using image difficulty prediction," in *Proc. IEEE 20th Int. Symp. Symbolic Numeric Algorithms Sci. Comput.*, 2018, pp. 209–214.

[30] I. Amin, A. J. Taylor, F. Junejo, A. Al-Habaibeh, and R. M. Parkin, "Automated people-counting by using low-resolution infrared and visual cameras," *Measurement*, vol. 41, no. 6, pp. 589–599, 2008.

[31] J.-H. Choi, J.-E. Kim, and K.-T. Kim, "Deep learning approach for radar-based people counting," *IEEE Internet Things J.*, vol. 9, no. 10, pp. 7715–7730, May 2022.

[32] T. Zheng, Z. Chen, C. Cai, J. Luo, and X. Zhang, "V2iFi: In-vehicle vital sign monitoring via compact RF sensing," *Proc. ACM Interact. Mob. Wearable Ubiquitous Technol.*, vol. 4, no. 2, Jun 2020. [Online]. Available: https://doi.org/10.1145/3397321

[33] B. Mrazovac, M. Z. Bjelica, D. Kukolj, B. M. Todorovic, and D. Samardzija, "A human detection method for residential smart energy systems based on ZigBee RSSI changes," *IEEE Trans. Consum. Electron.*, vol. 58, no. 3, pp. 819–824, Aug. 2012.

[34] Microphase AntSDR, 2021. [Online]. Available: https://github.com/MicroPhase/antsdr-fw

[35] R. W. Schafer, "What is a Savitzky-Golay filter?[Lecture notes]," *IEEE Signal Process. Mag.*, vol. 28, no. 4, pp. 111–117, Jul. 2011.

[36] F. Zhang et al., "Towards a diffraction-based sensing approach on human activity recognition," *Proc. ACM Interactive Mobile Wearable Ubiquitous Technol.*, vol. 3, no. 1, pp. 1–25, 2019.

[37] H. Wang, D. Zhang, J. Ma, Y. Wang, and B. Xie, "Human respiration detection with commodity WiFi devices: Do user location and body orientation matter?," in *Proc. ACM Int. Joint Conf. Pervasive Ubiquitous Comput.*, 2016, pp. 25–36.

[38] H. D. Hristov, *Fresnel Zones in Wireless Links, Zone Plate Lenses and Antennas*. Norwood, MA, USA: Artech House, Inc., 2000.

[39] G. and F., "The measure of fidget," *Nature*, vol. 32, no. 817, pp. 174–175, 1885.

[40] Y. Nam, Y. Kong, B. Reyes, N. Reljin, and K. H. Chon, "Monitoring of heart and breathing rates using dual cameras on a smartphone," *PLoS One*, vol. 11, no. 3, 2016, Art. no. e0151013.

[41] J. Birjandtalab, D. Cogan, M. B. Pouyan, and M. Nourani, "A non-EEG biosignals dataset for assessment and visualization of neurological status," in *Proc. IEEE Int. Workshop Signal Process. Syst.*, 2016, pp. 110–114.

[42] A. L. Goldberger et al., "PhysioBank, PhysioToolkit, and PhysioNet: Components of a new research resource for complex physiologic signals," *Circulation*, vol. 101, no. 23, 2000, Art. no. E215.

[43] K.-I. Goh and A.-L. Barabási, "Burstiness and memory in complex systems," *Europhysics Lett.*, vol. 81, no. 4, 2008, Art. no. 48002.

[44] Y. Wu, C. Zhou, J. Xiao, J. Kurths, and H. J. Schellnhuber, "Evidence for a bimodal distribution in human communication," *Proc. Nat. Acad. Sci. USA*, vol. 107, no. 44, pp. 18 803–18 808, 2010.

[45] W. Stadje, "The busy period of the queueing system m/g/," *J. Appl. Probability*, vol. 22, no. 3, pp. 697–704, 1985.

[46] C. A. Hidalgo R, "Conditions for the emergence of scaling in the inter-event time of uncorrelated and seasonal systems," *Physica A Meas. Mechanics Appl.*, vol. 369, no. 2, pp. 877–883, 2006.

[47] T. Zhou, Z.-D. Zhao, Z. Yang, and C. Zhou, "Relative clock verifies endogenous bursts of human dynamics," *Europhysics Lett.*, vol. 97, no. 1, 2012, Art. no. 18006.

[48] V. Trees and L. Harry, *Detection, Estimation, Modulation Theory, Part 1 - Detection, Estimation, Linear Modulation Theory*, New York, NY, USA: John Wiley & Sons, 2001.

Hongbo Jiang (Senior Member, IEEE) received the PhD degree from Case Western Reserve University in 2008. He is now a full professor with the College of Computer Science and Electronic Engineering, Hunan University. He was a professor with the Huazhong University of Science and Technology. His research concerns computer networking, especially algorithms and protocols for wireless and mobile networks. He is serving as the editor for *IEEE/ACM Transactions on Networking*, the associate editor for *IEEE Transactions on Mobile Computing*, and the associate technical editor for *IEEE Communications Magazine*.

Siyu Chen received the BS degree in communication engineering from Hunan University, Changsha, China. He is currently working toward the first-year PhD degree with the College of Computer Science and Electronic Engineer, Hunan University, China. His research interests include RF sensing and IoT security.

Zhu Xiao (Senior Member, IEEE) received the MS and PhD degrees in communication and information system from Xidian University, China, in 2007 and 2009, respectively. From 2010 to 2012, he was a research fellow with the Department of Computer Science and Technology, University of Bedfordshire, U.K. He is currently a full professor with the College of Computer Science and Electronic Engineering, Hunan University, China. His research interests include mobile communications, wireless localization, Internet of Vehicles, and trajectory data mining.
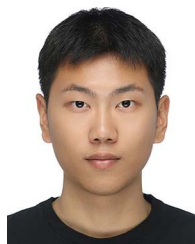
Jingyang Hu is currently working toward the second-year PhD degree with the College of Computer Science and Electronic Engineer, Hunan University, China. From 2022 to 2023, he works as a joint PhD degree with the School of Computer Science and Engineering, Nanyang Technological University (NTU), Singapore. He has published papers in ACM Ubicomp/IMWUT 2021, IEEE ICDCS 2022, etc. His research interests include RF sensing and deep learning.

Jiangchuan Liu (Fellow, IEEE) received the BEng (cum laude) degree in computer science from Tsinghua University, Beijing, China, in 1999, and the PhD degree in computer science from the Hong Kong University of Science and Technology, in 2003. He is currently a full professor (with University Professorship) with the School of Computing Science, Simon Fraser University, BC, Canada. He is a fellow of the Canadian Academy of Engineering and the NSERC E.W.R. Steacie Memorial fellow. He is a steering committee member of *IEEE Transactions on Mobile Computing*. He was a co-recipient of the Test of Time Paper Award of the IEEE INFOCOM, in 2015, the ACM TOMCCAP Nicolas D. Georganas Best Paper Award, in 2013, and the ACM Multimedia Best Paper Award, in 2012. He is an associate editor of the *IEEE/ACM Transactions on Networking*, the *IEEE Transactions on Big Data*, and the *IEEE Transactions on Multimedia*.

Schahram Dustdar (Fellow, IEEE) received the PhD degree in business informatics from the University of Linz, Austria, in 1992. He is currently a full professor of Computer Science (Informatics) with a focus on Internet Technologies heading the Distributed Systems Group, TUWien, Wein, Austria. He is currently a full professor of Computer Science (Informatics) with a focus on Internet Technologies heading the Distributed Systems Group, TU Wien, Wein, Austria. He is the Chairman of the Informatics Section of the Academia Europaea (since December 9, 2016). Dr. Dustdar is a member of the IEEE Conference Activities Committee (CAC) (since 2016), of the Section Committee of Informatics of the Academia Europaea (since 2015), and of the Academia Europaea: The Academy of Europe, Informatics Section (since 2013). He was the recipient of the ACM Distinguished Scientist Award (2009) and the IBM Faculty Award (2012). He is an associate editor for the *IEEE TRANSACTIONS ON SERVICES COMPUTING*, *ACM Transactions on the Web*, and *ACM Transactions on Internet Technology*, and on the editorial board of IEEE.